DRAFT VERSION NOVEMBER 7, 2012
Preprint typeset using LaTeX style emulateapj v. 08/22/09

KELT-3b: A HOT JUPITER TRANSITING A V=9.8 LATE-F STAR

JOSHUA PEPPER[1], ROBERT J. SIVERD[1], THOMAS G. BEATTY[2], B. SCOTT GAUDI[2], KEIVAN G. STASSUN[1,3], JASON EASTMAN[4,5], KAREN COLLINS[6], DAVID W. LATHAM[7], ALLYSON BIERYLA[7], LARS A. BUCHHAVE[8,9], ERIC L. N. JENSEN[10], MARK MANNER[11], KALOYAN PENEV[12], JUSTIN R. CREPP[13], PHILLIP A. CARGILE[1], SAURAV DHITAL[1,14], MICHAEL L. CALKINS[7], GILBERT A. ESQUERDO[7], PERRY BERLIND[7], BENJAMIN J. FULTON[4,15], RACHEL STREET[4], QINGQING MAO[1], ALEXANDER J. W. RICHERT[16], ANDREW GOULD[2,17], DARREN L. DEPOY[18], JOHN F. KIELKOPF[6], JENNIFER L. MARSHALL[18], RICHARD W. POGGE[2,17], ROBERT P. STEFANIK[7], MARK TRUEBLOOD[19], PATRICIA TRUEBLOOD[19],

Draft version November 7, 2012

ABSTRACT

We report the discovery of KELT-3b, a moderately inflated transiting hot Jupiter with a mass of $1.462^{+0.067}_{-0.066} M_J$, and radius of $1.358^{+0.068}_{-0.069} R_J$, with an orbital period of 2.703390 ± 0.000010 days. The host star, KELT-3, is a V = 9.8 late F star with $M_* = 1.282^{+0.062}_{-0.060} M_\odot$, $R_* = 1.482^{+0.062}_{-0.064} R_\odot$, $T_{\rm eff} = 6304 \pm 49$ K, log(g) = $4.204^{+0.031}_{-0.029}$, and [Fe/H] = $0.048^{+0.079}_{-0.081}$, and has a likely proper motion companion. KELT-3b is the third transiting exoplanet discovered by the KELT survey, and is orbiting one of the 20 brightest known transiting planet host stars, making it a promising candidate for detailed characterization studies. Although we infer that KELT-3 is significantly evolved, a preliminary analysis of the stellar and orbital evolution of the system suggests that the planet has likely always received a level of incident flux above the empirically-identified threshold for radius inflation suggested by Demory & Seager (2011).

Subject headings:

1. INTRODUCTION

Transiting extrasolar planets are the best laboratories for studying the individual properties of exoplanets, providing clues about planetary formation and evolution. Information about planetary mass, radius, atmosphere, and spin-orbit alignment can most easily be gathered from transiting exoplanets that orbit bright stars, since the greater flux from such stars enables faster, cheaper, and more precise follow-up observations.

The Kilodegree Extremely Little Telescope (KELT) transit survey is designed to find precisely these planets. The KELT-North telescope (Pepper et al. 2007) has a small aperture and wide field of view ($26^\circ \times 26^\circ$) to observe the entire sky between declinations 19°N and 45°N, covering approximately 40% of the northern sky. The aperture, optical system, and exposure time for KELT-North are configured to obtain better than 1% RMS photometry for stars with $8 < V < 10$. That magnitude range represents the brightness gap between comprehensive RV surveys and most other transit surveys.

The KELT-North survey has been operating since 2006, and we have been vetting transit candidates since April 2011. The first two KELT transit discoveries demonstrate the scientific potential of this effort. KELT-1b (Siverd et al. 2012) is a $27 M_J$ brown dwarf transiting a V=10.7 star. KELT-1 is the brightest star known to host a transiting brown dwarf. KELT-2Ab (Beatty et al. 2012) is a transiting hot Jupiter orbiting a V=8.77 star. KELT-2A, the brighter of two stars in a visual binary, is the ninth-brightest star known to harbor a transiting planet and the third-brightest discovered to date by a ground-based transit survey. In this paper we describe the discovery and characterization of a hot Jupiter transiting the bright V=9.8 star TYC 2996-683-1.

2. DISCOVERY AND FOLLOW-UP OBSERVATIONS

The KELT survey has an established process for reducing KELT survey data, extracting light curves, identifying potential transiting planets, and performing follow-up observations. We provide a brief summary of the KELT reductions in §2.1; for more details, see §2 of Siverd et al. (2012).

2.1. *KELT Observations and Photometry*

KELT-3 is in KELT-North survey field 06, which is centered on (α = 09h46m48s, δ = +31d44m37s; J2000). We monitored field 06 from October 27, 2006, to April 1, 2011, collecting

[1] Department of Physics and Astronomy, Vanderbilt University, Nashville, TN 37235, USA
[2] Department of Astronomy, The Ohio State University, Columbus, OH 43210, USA
[3] Department of Physics, Fisk University, Nashville, TN 37208, USA
[4] Las Cumbres Observatory Global Telescope Network, Santa Barbara, CA 93117, USA
[5] Department of Physics Broida Hall, University of California, Santa Barbara, CA 93106, USA
[6] Department of Physics & Astronomy, University of Louisville, Louisville, KY 40292, USA
[7] Harvard-Smithsonian Center for Astrophysics, Cambridge, MA 02138, USA
[8] Niels Bohr Institute, University of Copenhagen, 21S00 Copenhagen, Denmark
[9] Centre for Star and Planet Formation, Natural History Museum of Denmark, University of Copenhagen, DK-1350 Copenhagen, Denmark
[10] Department of Physics and Astronomy, Swarthmore College, Swarthmore, PA 19081, USA
[11] Spot Observatory, Nunnelly, TN 37137, USA
[12] Department of Astrophysical Sciences, Princeton University, Peyton Hall, Princeton, NJ 08544, USA
[13] Department of Physics, University of Notre Dame, Notre Dame, IN 46556, USA
[14] Department of Astronomy, Boston University, 725 Commonwealth Avenue, Boston, MA 02215, USA
[15] Institute for Astronomy, University of Hawaii, Honolulu, HI 96822, USA
[16] Astronomy and Astrophysics Department, Pennsylvania State University, University Park, PA, USA
[17] Center for Cosmology and Astroparticle Physics, The Ohio State University, OH 43210, USA
[18] Department of Physics & Astronomy, Texas A&M University, College Station, TX 77843, USA
[19] Winer Observatory, Sonoita, AZ 85637, USA

a total of 6,619 observations. We reduced the raw survey data using a custom implementation of the ISIS image subtraction package (Alard & Lupton 1998; Alard 2000), combined with point-spread fitting photometry using DAOPHOT (Stetson 1987). Using proper motions from the Tycho-2 catalog (Høg et al. 2000) and a reduced proper motion cut based on Collier Cameron et al. (2007), we selected likely dwarf and subgiant stars within the field for further post-processing and analysis. We applied the trend filtering algorithm (TFA; Kovács et al. 2005) to each remaining light curve to remove systematic noise, followed by a search for transit signals using the box-fitting least squares algorithm (BLS; Kovács et al. 2002). For both TFA and BLS we used the versions found in the VARTOOLS package (Hartman et al. 2008).

One of the candidates from field 06 was star BD+41 2024 / TYC 2996-683-1 / 2MASS J09543439+4023170, located at (α = 09h54m34.388s, δ = +40d23m16.98s; J2000). The star (henceforth KELT-3) has Tycho magnitudes B_T = 10.397 $\pm$ 0.032 and V_T = 9.873 $\pm$ 0.029 (Høg et al. 2000) (Johnson magnitudes B = 10.27 and V = 9.82), and passed our initial selection cuts. The discovery light curve of KELT-3 is shown in Figure 1. We observed a transit-like feature at a period of 2.70339 days, with a depth of about 10 mmag.

KELT-3 has a faint (r = 13.3) nearby stellar neighbor about 3.7 arcseconds to the northeast, SDSS7 J095434.58+402319.6 (SDSS-DR7; Adelman-McCarthy & et al. 2009). The presence of this object (henceforth SDSS7J095434) complicates some of our analysis, which we address in §3.5.

2.2. *Radial-Velocity Observations*

After KELT-3 was selected as a candidate, we conducted radial-velocity (RV) observations to identify possible false-positive signatures and to determine the RV orbit. We obtained data using the Tillinghast Reflector Echelle Spectrograph[20] (TRES; Fűrész 2008), on the 1.5m Tillinghast Reflector at the Fred L. Whipple Observatory (FLWO) at Mt. Hopkins, AZ. We observed KELT-3 sixteen times with TRES over two months, from UT February 26, 2012, to UT May 2, 2012. The spectra had a resolving power of R=44,000, and were extracted following the procedures described by Buchhave et al. (2010).

We also observed KELT-3 with the FIbre-fed Echelle Spectrograph (FIES) on the 2.5 m Nordic Optical Telescope (NOT) in La Palma, Spain (Djupvik & Andersen 2010). We acquired 5 FIES spectra between 13 and 17 March 2012 with the high–resolution fiber (1.″3 projected diameter) with resolving power of R $\approx$ 67,000, and wavelength coverage of $\sim$3600-7400 Å. We used the wavelength range from approximately 4000-6100 Å to determine the radial velocities. The exposure times ranged from 7 to 15 minutes, yielding a SNR from 31 to 52 pixel^{-1} (SNR of 49 to 83 per resolution element) in the wavelength region containing the Mgb triplet. The procedures used to reduce the FIES spectra and extract the radial velocities are those described in Buchhave et al. (2010) and the spectral classification of the FIES spectra is described in Buchhave et al. (2012). Both the TRES and FIES observations were conducted with fibers smaller than 1.5 arcseconds, so that there is no expected contamination from SDSS7J095434, which is about 3.7 arcseconds away.

Table 1 lists all RV data for KELT-3, and Figure 2 shows the RV data phased to the orbit fit, along with the residuals to the model fit and the bisector spans. We find the RMS of the bisector spans to be 13.2 m s^{-1}, which is significantly lower than the RV semi-amplitude of 179.6 m s^{-1}. The absence of a trend and low RMS of the bisector spans in phase suggests that the measured RV variations are due to real RV variations in the target star.

TABLE 1
RV OBSERVATIONS OF KELT-3

BJD (TDB)	RV (m s^{-1})	RV error[a] (m s^{-1})	Source
2455983.672916	-319	25	TRES
2455990.777987	-66	14	TRES
2456000.473809	-31	27	FIES
2456001.465355	103	20	FIES
2456002.514673	-259	20	FIES
2456003.552533	90	16	FIES
2456004.432251	0	16	FIES
2456018.656206	-324	14	TRES
2456019.709404	4	19	TRES
2456020.710562[b]	-125	18	TRES
2456021.776310	-282	10	TRES
2456022.786222	0	10	TRES
2456023.806566	-293	13	TRES
2456024.741118	-173	19	TRES
2456025.668112	2	18	TRES
2456026.816586	-334	14	TRES
2456029.644415	-357	13	TRES
2456033.837821	21	20	TRES
2456045.694187	-333	15	TRES
2456048.634878	-331	23	TRES
2456049.760849	22	21	TRES

[a]Unrescaled measurement errors.
[b]This observation occured during transit and was excluded from the EXOFAST analysis in §3.5.

2.3. *Follow-up Time-Series Photometry*

We acquired follow-up time-series photometry of KELT-3 to check for other types of false positives and to better determine the transit shape. We obtained eight partial or full transits in multiple bands between March and June 2012. For all instruments except FTN, the faint neighbor SDSS7J095434 was included in the photometric aperture, and so the resultant light curves include both KELT-3 and SDSS7J095434. Figure 3 shows all the follow-up light curves assembled. We find the same R_P/R_* ratio in all light curves, which include observations in the *g*, *r*, *i*, and Pan-Starrs-*Z* filters[21], helping to rule out false positives due to blended eclipsing binaries.

We observed two transits of KELT-3 at Swarthmore College's Peter van de Kamp Observatory. The observatory uses a 0.6m RCOS telescope with an Apogee U16M 4K $\times$ 4K CCD, giving a 26' $\times$ 26' field of view. Using 2 $\times$ 2 binning, it has 0.76 arcseconds pixel^{-1}. On UT 2012-03-17 we obtained a partial transit including egress in *r*. On UT 2012-04-13 we observed an entire transit in *g*.

We observed two transits of KELT-3 at Moore Observatory, operated by the University of Louisville. We used the 0.6m RCOS telescope with an Apogee U16M 4K $\times$ 4K CCD, giving a 26' $\times$ 26' field of view and 0.39 arcseconds pixel^{-1}. The data were calibrated with the AstroImageJ package (Collins, et al., in preparation). On UT 2012-04-02 we obtained a full transit in *i*, although observing conditions created some interruptions in the data. On UT 2012-06-07 we obtained a nearly-

[20] http://tdc-www.harvard.edu/instruments/tres/

[21] In all references to SDSS filters in this paper, we use the unprimed notation, to denote generic SDSS-like filters, which in practice are often labeled with the primed notation.

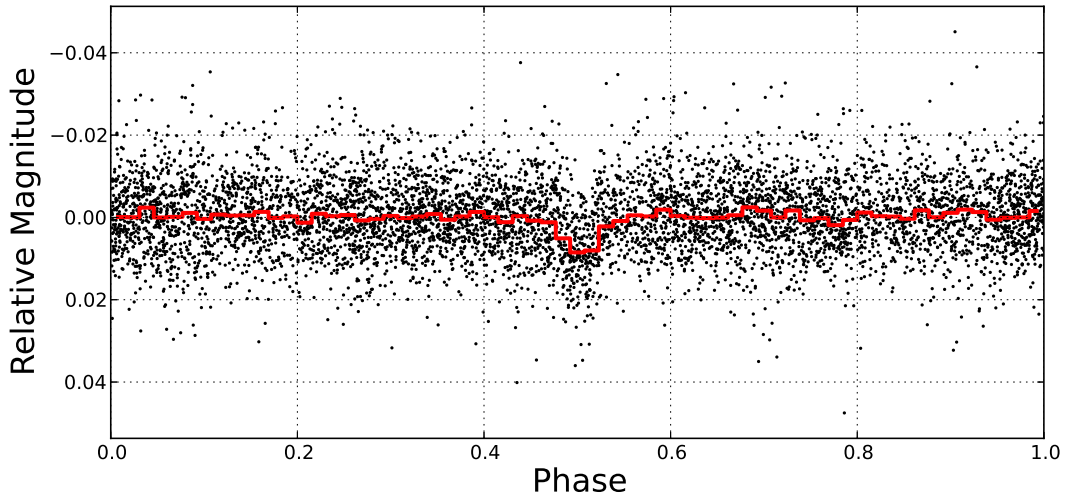

FIG. 1.— Discovery light curve of KELT-3b from the KELT-North telescope. The light curve contains 6,619 observations spanning 4.4 years, phase-folded to the orbital period of 2.70339 days. The red line represents the same data binned at 1-hour intervals in phase.

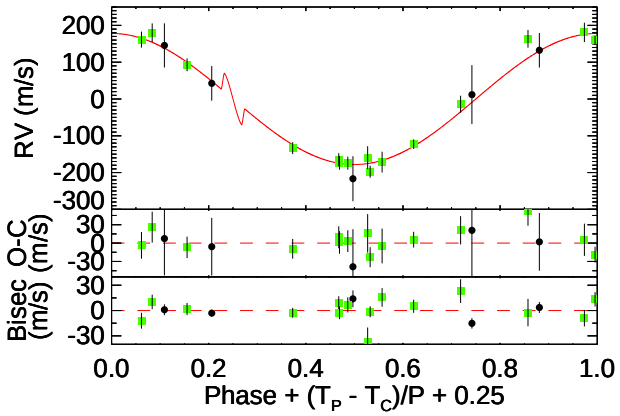

FIG. 2.— Radial velocity measurements of KELT-3 from both TRES and FIES. *Top panel:* RV observations phased to our best orbital model with eccentricity fixed to zero and with no linear trend, shown in red. TRES observations are shown in green, while FIES observations are in black, and the error bars are scaled according to the method described in §3.5. The RV observation taken during transit is not plotted. The predicted Rossiter-McLaughlin effect in the model shown incorporates an assumption that $\lambda = 0$ (i.e. that the projected spin-obit alignment of the system is 0 degrees). *Middle panel:* Residuals of the RV observations to our circular orbital fit. *Bottom panel:* Bisector span of each observation as a function of phase.

full transit in *r*.

We observed two transits with Faulkes Telescope North (FTN), operated by Las Cumbres Observatory Global Telescope (LCOGT). FTN is a 2.0m telescope with a 4K × 4K Spectral camera, and we bin the transit observations in 2 × 2 mode. On UT 2012-04-02 we obtained a partial transit in Pan-Starrs-*Z*, which includes most of the in-transit phase plus the full egress. On UT 2012-04-12 we obtained a full transit in Pan-Starrs-*Z*. Both observations were able to resolve KELT-3 from SDSS7J095434.

We observed a full transit from Byrne Observatory at Sedgwick (BOS), also operated by LCOGT. BOS is an 0.8m telescope with an 3K × 2K SBIG STL-6303E camera with 0.572 arcseconds pixel^{-1} and a 14.7' × 9.8' field of view. On UT 2012-04-03 we obtained a full transit in *g*, using 2 × 2 binning.

We observed a full transit in *i* on UT 2012-04-03 with KeplerCam on the 1.2m telescope at FLWO. KeplerCam has a single 4K × 4K Fairchild CCD with 0.366 arcseconds pixel^{-1}, and a field of view of 23.1' × 23.1'. The data were reduced using procedures outlined in Carter et al. (2011), which uses standard IDL routines.

2.4. *Single-epoch Multiband Photometry of SDSS7J095434*

In an effort to better characterize the relative colors and magnitudes of KELT-3 and SDSS7J095434, we observed the stars with FTN on UT 2012-04-02 in good conditions in the *g*, *r*, *i* and Pan-Starrs-*Z* filters. We find that the neighbor has $g = 14.05 \pm 0.23$, $r = 13.35 \pm 0.17$, $i = 12.85 \pm 0.17$, and $PS-Z = 12.48 \pm 0.19$.

2.5. *Adaptive Optics Observations*

In order to better assess the nature of SDSS7J095434 and search for any other faint neighbors, we obtained adaptive optics images using NIRC2 (instrument PI: Keith Matthews) at Keck on UT 2012-05-07. Our observations consist of dithered frames taken with the *K*' and *J* filters. We used the narrow camera setting to provide fine spatial sampling of the stellar point-spread function, and used KELT-3 as its own on-axis natural guide star. The total on-source integration time was 16.3 seconds in each bandpass. The resulting *K*' image is shown in Figure 5.

We find no other faint neighbors in the immediate vicinity of KELT-3. Specifically, we can exclude additional companions beyond a distance of 0.5 arcseconds from KELT-3 down to a magnitude difference of 6.5 magnitudes at 10–σ confidence. The magnitude differences between KELT-3 and SDSS7J095434 are $\Delta J = 3.001 \pm 0.019$ mag, and $\Delta K' = 2.436 \pm 0.014$ mag. The angular separation between the stars is 3724 ± 1 mas and the position angle of SDSS7J095434 is 42.00 ± 0.03 degrees, measured east of North.

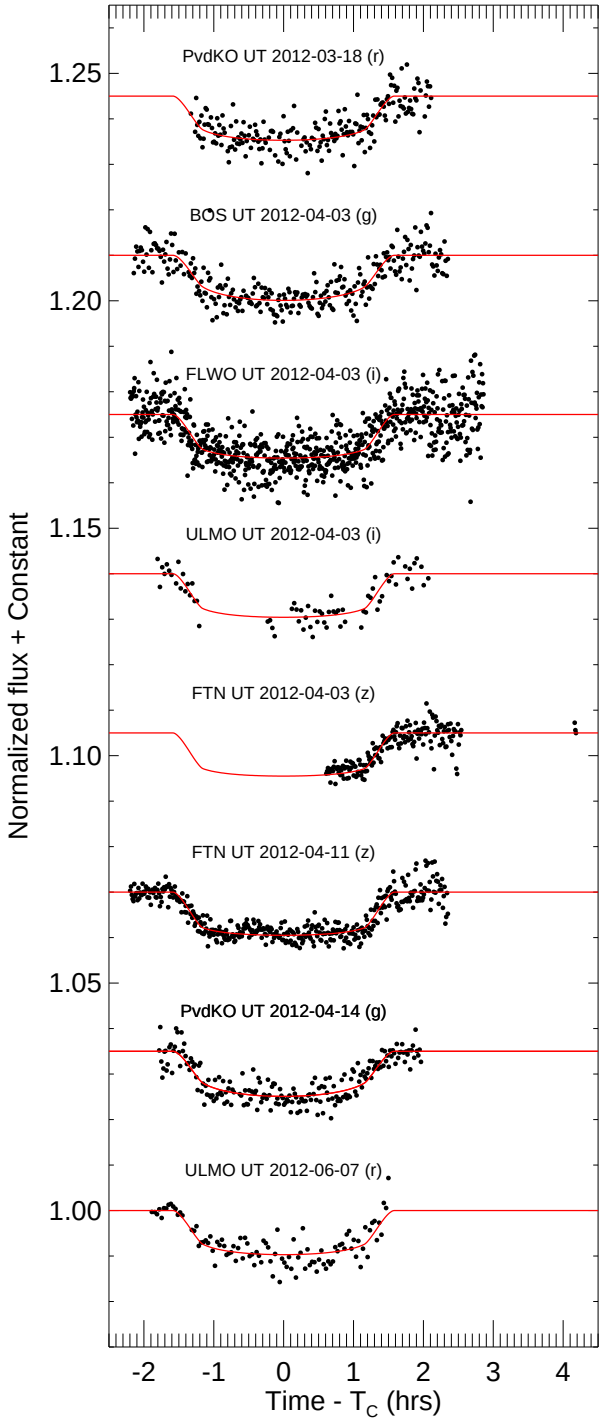

FIG. 3.— Follow-up transit photometry of KELT-3. The red overplotted lines are the best fit transit model. The labels are as follows: PvdKO - Peter van de Kamp Observatory (Swarthmore); ULMO - University of Louisville Moore Observatory; FTN - Faulkes Telescope North (LCOGT); BOS - Byrne Observatory at Sedgwick (LCOGT); FLWO - KeplerCam at Fred L. Whipple Observatory.

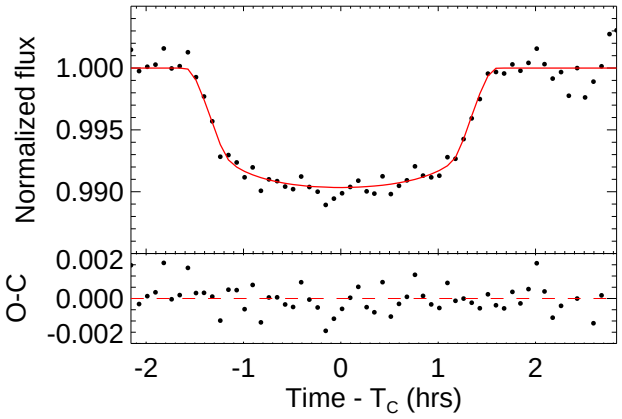

FIG. 4.— *Top panel:* All follow-up light curves from Figure 3, combined and binned in 5 minute intervals. This light curve is not used for analysis, but rather to show the best combined behavior of the transit. The red curve shows the six transit models for each of the individual fits combined and binned in 5 minute intervals the same way as the data, with the model points connected. *Bottom panel:* The residuals of the binned light curve from the binned model in the top panel.

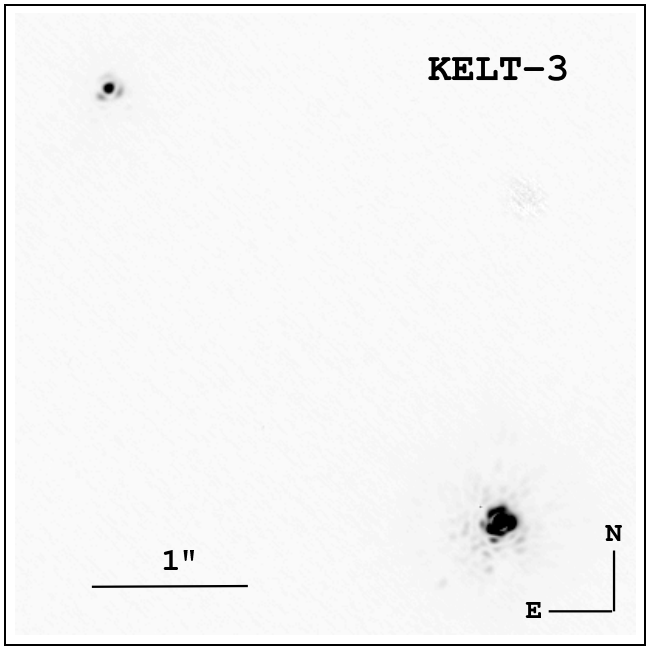

FIG. 5.— Keck adaptive optics image of KELT-3 taken with NIRC2 in the K' filter. KELT-3 is in the lower right corner of the panel, while the nearby star SDSS7J095434 is in the upper right, located 3.742 ± 0.001 arcseconds to the north east.

3. SYSTEM PARAMETERS AND FITS

3.1. *Spectroscopic Analysis*

We use both the TRES and FIES spectra to derive the stellar properties of KELT-3. Using the Spectral Parameter Classification (SPC) procedure (Buchhave et al., in preparation), we obtained stellar parameters from the average of all 16 TRES spectra, and separately from all 5 FIES spectra. Since each dataset yielded similar results, we combined the data from all 21 spectra, which yielded from SPC the following results: $T_{\rm eff} = 6308 \pm 50$ K, log(g) = 4.23 ± 0.10, [m/H] = 0.04 ± 0.08, and $V_{\rm rot} = 10.2 \pm 0.5$ km s^{-1}, giving the star an inferred spectral type of F7V. Based on those results, we are able to calculate the stellar mass and radius from the relations of Torres et al. (2010). In this case, we used [m/H] as a substitute for [Fe/H], but we do not believe that the difference should affect the results. We find that $M_* = 1.28 \pm 0.12 M_\odot$, and $R_* = 1.44 \pm 0.21 R_\odot$.

3.2. *SED Analysis*

We construct an empirical spectral energy distribution (SED) of KELT-3 using the FUV and NUV bandpasses from GALEX (Martin et al. 2005), the B_T and V_T colors from the Tycho-2 catalog (Høg et al. 2000), near-infrared (NIR) fluxes in the J and H passbands from the 2MASS Point Source Catalog (Cutri et al. 2003; Skrutskie et al. 2006), and near- and mid-IR fluxes in the four WISE passbands (Wright et al. 2010), to derive the SED shown in Figure 6. We fit this SED to NextGen models from Hauschildt et al. (1999) by fixing the values of $T_{\rm eff}$, log(g) and [Fe/H] inferred from the global fit to the light curve and RV data as described in §3.5 and listed in Table 4 for the circular orbit, and then finding the values of the visual extinction A_V and distance d that minimize χ^2. We find $A_V = 0.02 \pm 0.02$ and $d = 178 \pm 16$ pc. We note that the quoted statistical uncertainties on A_V and d are likely to be underestimated because we have not accounted for the uncertainties in values of $T_{\rm eff}$, log(g) and [Fe/H] used to derive the model SED. Furthermore, it is likely that alternate model atmospheres would predict somewhat different SEDs and thus values of the extinction and distance.

We also evaluate the motion of KELT-3 through the Galaxy to place it among standard stellar populations. The RV observations show that it has a bulk radial velocity of $+27.9 \pm 0.2$ km s^{-1}. Combining that with the distance and proper motion information from the NOMAD catalog (Zacharias et al. 2004), we find that KELT-3 has 3-space motion of U,V,W (where positive U is in the direction of the Galactic center) of -34.1 ± 1.6, -24.4 ± 2.2, 8.1 ± 1.3, all in units of km s^{-1}, making it a thin disk star.

While nearly all the details of this analysis appear consistent, one property that does not fit is the FUV flux of the system from GALEX. That flux is about 2 orders of magnitude higher than expected for the otherwise well-matched SED of KELT-3. We checked the signatures of chromospheric activity in KELT-3 from the spectroscopic observations, but we find no visible emission in the cores of the Ca-II H and K absorption lines, suggesting an essentially inactive star. That analysis is shown in Figure 7. The observed spectrum is compared with a synthetic spectrum generated using SME (Valenti & Piskunov 1996; Valenti & Fischer 2005) based on the stellar parameters from §3.5, model atmospheres from Kurucz (1992), and the line list from Kupka et al. (2000). The measured FUV excess is also inconsistent with the relationships found by Findeisen et al. (2011) between R'_{HK} and FUV-V excess and also between FUV-J and age (using the age of 3.0 Gyr determined in §3.3 below).

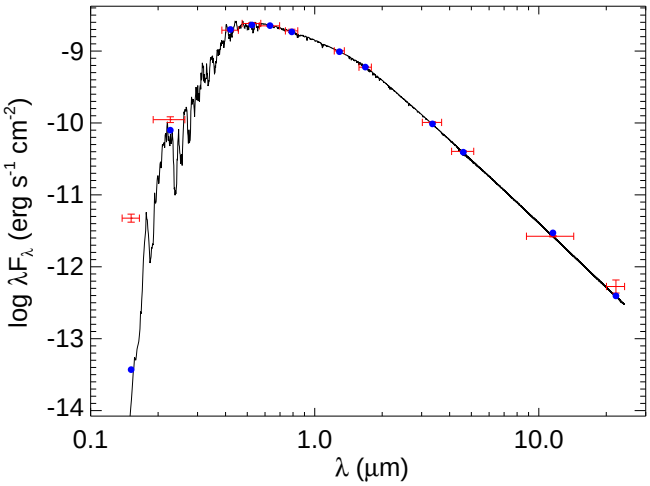

FIG. 6.— Measured and best-fit SED for KELT-3 from UV through NIR. The red errorbars indicate measurements of the flux of KELT-3 in UV, optical, and NIR passbands listed in Table 2. The vertical errorbars are the 1–σ photometric uncertainties, whereas the horizontal errorbars are the effective widths of the passbands. The solid curve is the best-fit theoretical SED from the NextGen models of Hauschildt et al. (1999), assuming stellar parameters $T_{\rm eff}$, log(g) and [Fe/H] fixed at the values in Table 4 from the circular fit, with A_V and d allowed to vary. The blue dots are the predicted passband-integrated fluxes of the best-fit theoretical SED corresponding to our observed photometric bands.

The PSF of GALEX has a 5-arcsecond FWHM, and is centered to within 0.6 arcseconds of KELT-3, with an approximate positional error of one to two arcseconds. Thus, KELT-3 is partially blended with the neighbor star SDSS7J095434 in the UV measurements, presenting the possibility that SDSS7J095434 is the source of the UV signal. However, aside from the better positional matching of the GALEX observations to KELT-3, the fainter V-magnitude of SDSS7J095434 leads to a FUV excess even more difficult to accommodate (assuming a stellar SED for SDSS7J095434).

An alternate possibility we consider is that since we do not have standard proper motions for SDSS7J095434, it is possibly not a star but a background AGN, which could explain the UV excess. We searched to see whether SDSS7J095434 was detected in the ROSAT or Fermi catalogs, or in catalogs of known radio sources, and did not find any detections. Also, with a measured brightness of $r = 13.3$, it would be extremely bright for an AGN or QSO. Furthermore, we perform several tests below in §3.4 and the Appendix, including a novel proper motion analysis, which strongly hint that SDSS7J095434 is most likely to be a star associated with KELT-3, disproving its AGN status.

We thus do not have an explanation for the excess FUV flux anomaly at this time, although we plan to investigate that issue further.

3.3. *Evolutionary Analysis*

In Figure 8 we plot the predicted evolutionary track of KELT-3 on a theoretical HR diagram (log(g) vs. $T_{\rm eff}$), from the Yonsei-Yale stellar models (Demarque et al. 2004). Here we have used the stellar mass and metallicity derived from the global circular orbit fit (§3.5 and Table 4). We also show evolutionary tracks for masses corresponding to the ± 1–σ ex-

TABLE 2
STELLAR PROPERTIES OF KELT-3

Parameter	Description (Units)	Value	Source	Reference
Names		BD+41 2024		
		TYC 2996-683-1		
		2MASS J09543439+4023170		
		GSC 02996-00683		
		SAO 43097		
α_{J2000}		09 54 34.391	Tycho-2	1
δ_{J2000}		+40 23 16.98	Tycho-2	1
FUV_{GALEX}		17.95 ± 0.14	GALEX	2
NUV_{GALEX}		14.09 ± 0.01	GALEX	2
B_T		10.397 ± 0.032	Tycho-2	1
V_T		9.873 ± 0.029	Tycho-2	1
r_{SDSS}		9.728 ± 0.015	Carlsberg	3
I_C		9.263 ± 0.057	TASS	4
J		8.963 ± 0.019	2MASS	5
H		8.728 ± 0.019	2MASS	5
WISE1		11.26 ± 0.022	WISE	6
WISE2		11.923 ± 0.019	WISE	6
WISE3		13.874 ± 0.023	WISE	6
WISE4		14.918 ± 0.227	WISE	6
μ_α	Proper Motion in RA (mas yr^{-1})	-28.9 ± 0.6	NOMAD	7
μ_δ	Proper Motion in Dec (mas yr^{-1})	-25.1 ± 0.7	NOMAD	7
U[a]	km s^{-1}	-34.1 ± 1.6	This paper	
V	km s^{-1}	-24.4 ± 2.2	This paper	
W	km s^{-1}	8.1 ± 1.3	This paper	
d	Distance (pc)	178 ± 16	This paper	
	Age (Gyr)	3.0 ± 0.2	This paper	
A_V	Visual Extinction	0.02 ± 0.02	This paper	

REFERENCES. — 1=Høg et al. (2000); 2=Martin et al. (2005); 3=Copenhagen University et al. (2006); 4=Richmond et al. (2000); 5=Cutri et al. (2003); Skrutskie et al. (2006); 6=Wright et al. (2010); Cutri et al. (2012); 7=Zacharias et al. (2004)

[a] Positive U is in the direction of the Galactic Center.

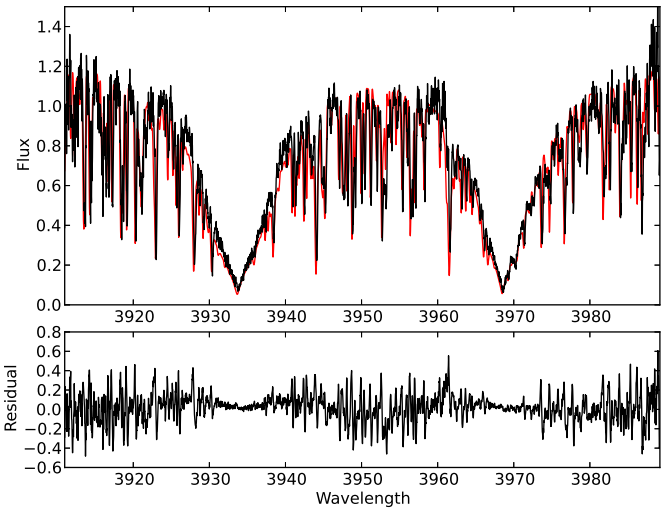

FIG. 7.— No evidence is seen for chromospheric activity in the spectrum of KELT-3. *Upper Panel*: The black curve shows the combined spectra for KELT-3 from the FIES observations, while the red line shows a synthetic spectrum generated using SME. The spectral range encompasses the Ca H and Ca K absorbtion lines, and no emission is seen in the core from either spectrum, consistent with no signs of chromospheric activity in KELT-3. *Lower Panel*: Residuals between the observed and synthetic spectra. The scatter in this plot mostly comes from missing line information in the line list for the synthetic spectrum and not noise in either spectrum. The noise level can be seen in the central parts of the Ca lines.

trema in the estimated uncertainty. We compare our $T_{\rm eff}$ and log(g) values and associated uncertainties to these tracks to estimate the age of KELT-3. These intersect the evolutionary track around 3.0 ± 0.2 Gyr.

To check that the isochrone age is consistent with the other parameters of KELT-3, we calculate the rotation period of the star, using the projected rotational velocity from §3.1 and the stellar radius from the full EXOFAST analysis in §3.5. Based on that rotation period of $P_{rot} \sin i = 7.11 \pm 0.54$ days, and the colors of the star, we calculate the predicted age from the models of Barnes (2007), which comes to 2.3 ± 0.7 Gyr, which is fully consistent with the isochrone age. We also checked the KELT light curve for periodic variability associated with spot modulation as an independent measure of P_{rot}, but we were unable to detect any significant sinusoidal variability beyond the photometric noise.

3.4. *Characterizing the Faint Neighbor SDSS7J095434*

Although SDSS7J095434 is identified in the SDSS catalog, its proximity to the much brighter KELT-3 means that the SDSS catalog magnitudes are unreliable, necessitating the new photometric measurements we obtained for this star listed in §2.4. Based on those measurements and the flux ratios in §2.5, we are able to construct an SED for SDSS7J095434 (Figure 9). We follow the same procedure described in §3.2. Since we do not have independent measures of $T_{\rm eff}$, log(g), and [Fe/H], in this case we let those three parameters vary, along with A_V and d, although we limit the maximal value of A_V to 0.04 mag, which is the line-of-sight value based on the dust maps in Schlegel et al. (1998). The colors of SDSS7J095434 suggest it is a K3 star with $T_{\rm eff} = 4800 \pm 400$K, and $A_V = 0.02 \pm 0.02$. The corresponding distance for such a star with the observed apparent magnitude, assuming it is a dwarf, is 265^{+47}_{-40} pc, compared to a distance of 178 ± 16 pc for KELT-3. If SDSS7J095434 is rather a subgiant or giant star, it is located at a much further distance and

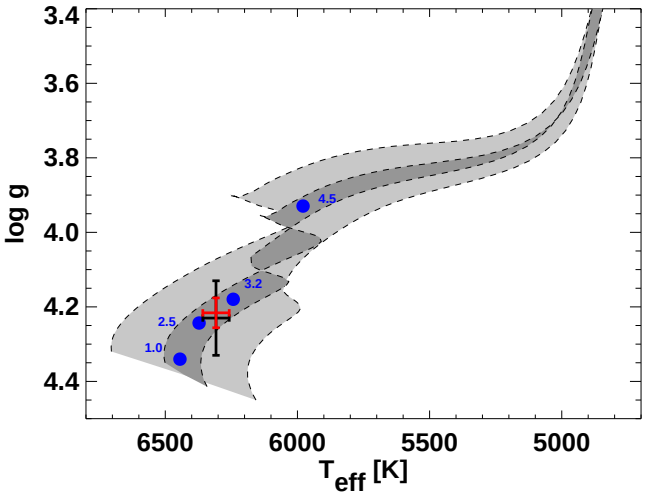

FIG. 8.— Theoretical HR diagram based on Yonsei-Yale stellar evolution models (Demarque et al. 2004). The gray swaths represent the evolutionary track for the best-fit values of the mass and metallicity of the host star from the circular joint fit described in §3.5, $M_* = 1.282^{+0.062}_{-0.060} M_\odot$ and [Fe/H] $=0.048^{+0.079}_{-0.081}$ (dark shaded), and from the spectroscopic constraints alone (light shaded). The tracks for the extreme range of the 1–σ uncertainties on M_* and [Fe/H] from the final analysis are shown as dashed lines bracketing each gray swath. The red cross shows the best-fit $T_{\rm eff} = 6304 \pm 49$K and $\log(g) = 4.204^{+0.031}_{-0.029}$ from the final EXOFAST analysis. The black cross shows the inferred $T_{\rm eff}$ and log(g) from the spectroscopic analysis alone. The blue dots represent the location of the star for various ages in Gyr. The host star is slightly evolved with a probable age of 3.0 ± 0.02 Gyr.

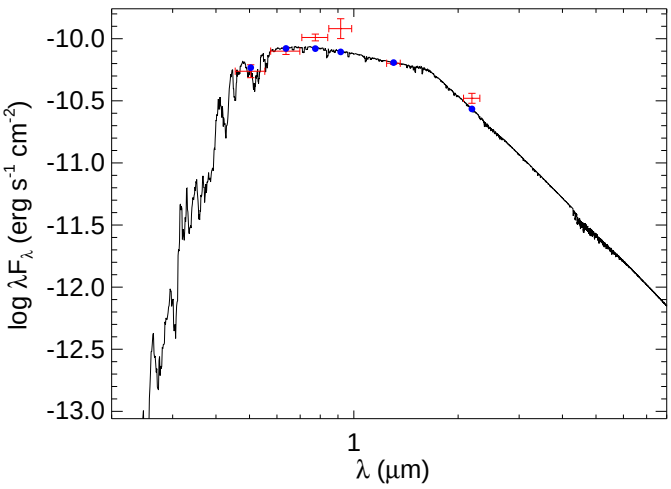

FIG. 9.— SED fit for SDSS7J095434, similar to Figure 6. The red errorbars indicate measurements of the flux of SDSS7J095434 listed in §2.4 and §2.5. The vertical errorbar indicates the photometric uncertainty, whereas the horizontal errorbar indicates the effective width of the passband. The solid curve is the best-fit theoretical SED from the NextGen models of Hauschildt et al. (1999). The blue dots are the predicted passband-integrated fluxes of the best-fit theoretical SED.

thus certainly unassociated with KELT-3. Although the calculated distances to SDSS7J095434 and KELT-3 are not the same, the uncertainties in the distances allow for some chance that they are associated. If we compare the distances and assume that the calculated errors are Gaussian, we find that there is a 1.76% probability that the values are consistent, assuming SDSS7J095434 is a dwarf star.

Because of the presence of the FUV excess, and the marginal evidence for the consistent distances for KELT-3 and SDSS7J095434, we perform a number of tests to investigate the nature of SDSS7J095434 and its association with KELT-3. That analysis is included in the Appendix, and includes a proper motion analysis that tentatively rules out the AGN nature of SDSS7J095434, indicating that it is a dwarf star physically associated with KELT-3. Based on the proper motion of KELT-3, we will be able to solidify that conclusion within the next year after obtaining additional high-precision astrometry of both sources to determine their relative proper motion.

3.5. *EXOFAST Analysis*

To determine the final orbital and physical parameters of the KELT-3 system, we use the results from the spectroscopic and SED analyses, the light curves, and the RVs of KELT-3 as inputs to EXOFAST (Eastman et al. 2012), which does a simultaneous Markov Chain Monte Carlo (MCMC) analysis of the entire system, including constraints on the stellar parameters M_* and R_* from the empirical relations in Torres et al. (2010). This method is similar to that described in detail in Siverd et al. (2012), but we note a few differences below.[22]

We scale the errors on the RV data such that the probability that the χ^2 was larger than the value we achieved, $P(>\chi^2)$ was 0.5 so as to ensure the resulting parameter uncertainties were roughly accurate. We must do that process separately for the TRES and FIES RV observations, and since there are not enough observations from FIES to perform an independent fit, we fit the TRES data independently, scale their errors so $P(\chi^2) = 0.5$, then iteratively scale the FIES errors until the combined $P(\chi^2) = 0.5$. In addition, one of the TRES RVs landed during transit, which we discarded so as not to be biased by the Rossiter-McLaughlin effect.

In this analysis, a complication arises because the light from KELT-3 and SDSS7J095434 was blended in all light curves except those from FTN. As in our analysis of KELT-2Ab (Beatty et al. 2012), which describes the process in more detail, we iteratively used the primary properties inferred from the full EXOFAST fit, combined with the model SED of the neighbor, to model and subtract the contribution of the flux from the neighbor in all the blended light curves.

The stellar and planetary parameters derived from this procedure are shown in Table 4. We see no evidence for a significant slope in the RV data – leaving the RV slope as a parameter to fit in the EXOFAST analysis yields a slope of 0.01 ± 0.35 m s^{-1} day^{-1}. After computing the fit with the slope fixed to zero, we find that the orbital parameters show a small but nominally significant (at $\sim$2–σ) non-zero eccentricity. As in the analysis from Beatty et al. (2012), the nearly zero values for $e\cos\omega_*$ and $e\sin\omega_*$ suggest that the non-zero eccentricity we find is due to Lucy-Sweeney eccentricity bias (Lucy & Sweeney 1971). We therefore compute a second EXOFAST fit in which both the orbital eccentricity and the RV slope are fixed to zero. With that fit, we end up scaling the TRES RV errors by 1.23, and the FIES errors by 2.99. Using the error-scaled data, we obtain an RMS of the RV residuals

[22] In the EXOFAST analysis, which includes the modelling of the filter-specific limb darkening parameters of the transit, we employ the transmission curves defined for the primed SDSS filters rather than the unprimed versions. We expect any differences due to that discrepancy to be well below the precision of all our observations in this paper and of the limb darkening tables from Claret & Bloemen (2011).

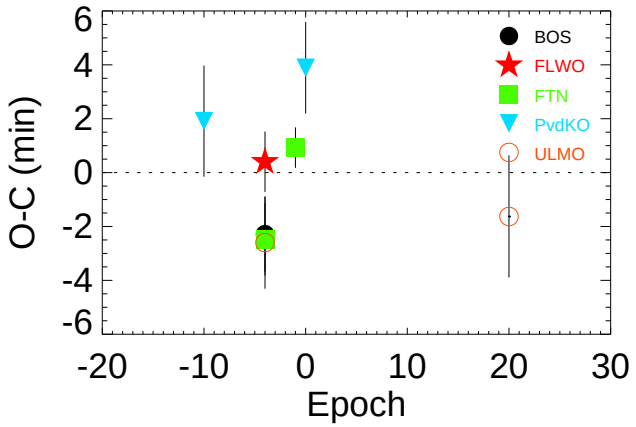

FIG. 10.— The residuals of the transit times from the best-fit ephemeris. The transit times are given in Table 3.

from the TRES data of 17.9 m s^{-1}, and for the FIES data an RMS of 20.5 m s^{-1}. We also compute the RMS of the bisectors, obtaining an RMS of 14.5 m s^{-1} from the TRES data, and an RMS of 10.6 m s^{-1} from the FIES data.

We investigate the residuals of the circular fit for any signs of transit time variations (TTVs). When we fit the transits shown in Table 3, the constraints on T_C and P only come from the RV and the prior imposed from the KELT discovery data, not the follow up light curves. Using the transit times to constrain the period during the fit would artificially reduce any observed TTV signal. We fit a straight line to all mid transit times, listed in Table 3 and plotted in Figure 10, to derive a separate ephemeris from only the transit data: $T_0 = 2456031.59122 \pm 0.00035$, $P = 2.703471 \pm 0.000065$, with a χ^2 of 15.57 and 6 degrees of freedom. While the χ^2 is slightly larger than one would naively expect, this is often the case in TTV studies, likely due to small systematics in the transit data. The largest deviation from the linear ephemeris is only slightly more than 2–σ, so we conclude there is no convincing evidence for TTVs.

The final system parameters found for KELT-3, based on the circular, no-slope fit, are $M_* = 1.282^{+0.062}_{-0.060} M_\odot$, $R_* = 1.482^{+0.062}_{-0.064} R_\odot$, $T_{\rm eff} = 6304 \pm 49$ K, log(g) = $4.204^{+0.031}_{-0.029}$, [Fe/H] = $0.048^{+0.079}_{-0.081}$. The planet is an inflated hot Jupiter with $M_P = 1.462^{+0.067}_{-0.066} M_J$, $R_P = 1.358^{+0.068}_{-0.069} R_J$. It is strongly irradiated, with an equilibrium temperature of $T_{\rm eq} = 1821^{+35}_{-37}$ K and an incident flux of $2.50 \pm 0.20 \times 10^9$ erg s^{-1} cm^{-2}. The radius is about 25% larger than predicted from the models of Baraffe et al. (2008) for an irradiated planet with a mass of 1 to 2 M_J at 3 Gyr and a small amount of metals.

TABLE 3
TRANSIT TIMES FOR KELT-3

Telescope and filter	Epoch	T_C (BJD_{TDB})	Error (seconds)	O-C (seconds)	(O - C)/Error
PvdKO, *r*	-10	2456004.557840	125	114.20	0.91
BOS, *g*	-4	2456020.775759	85	-136.73	-1.60
FLWO, *i*	-4	2456020.777589	69	21.38	0.31
ULMO, *i*	-4	2456020.775479	103	-160.92	-1.56
FTN, *z*	-4	2456020.775727	81	-139.50	-1.71
FTN, *z*	-1	2456028.888411	47	56.84	1.19
PvdKO, *g*	0	2456031.593592	93	204.62	2.19
ULMO, *r*	20	2456085.659456	139	-101.84	-0.73

4. BACKTRACKING THE EVOLUTION OF KELT-3

KELT-3b is somewhat inflated, with a density of $0.721^{+0.11}_{-0.090}$ g cm^{-3}. In an investigation of transiting giant exoplanets, Demory & Seager (2011) found that exoplanets that are insolated beyond a certain threshold (2×10^8 erg s^{-1} cm^{-2}) have radii that are inflated compared to those planets with lower levels on insolation. KELT-3b falls well above that threshold, and follows the insolation-inflation trend displayed in Figure 1 of Demory & Seager (2011). It is worth investigating, however, whether that relationship has always held true. That is, has KELT-3b always been as insolated as it is now? If it turns out that KELT-3b only recently began receiving enhanced irradiation, this could provide an empirical probe of the timescale of inflation mechinisms (see Assef et al. (2009) and Spiegel & Madhusudhan (2012)).

In order to answer that question, we simulate the reverse-evolution of the star-planet system, using the measured parameters listed in this paper as the present boundary conditions. This analysis is not intended to examine circularization of the planet, tidal locking to the star, or any type of planet-planet or planet-disk migration. Rather, it is a way to measure the insolation of the planet over time due to the changing luminosity of the star and changing star-planet separation.

We include the evolution of the star, assumed to follow the YREC $1.3 M_\odot$ model with solar metallicity (Siess et al. 2000). We assume that the stellar rotation was influenced only by tidal torques due to the planet, with no magnetic wind and treating the star like a solid body. We also assume a circular orbit throughout the full analysis. The results of our simulations are shown in Figure 11. We tested a range of values for the tidal quality factor of the star $Q_\star$, from log($Q_\star$) = 5 to log($Q_\star$) = 9. We find that although for certain values of $Q_\star$ the planet has moved substantially closer to its host during the past Gyr, in all cases the planet has always received more than enough flux from its host to keep the planet irradiated beyond the insolation threshold identified by Demory & Seager (2011). The rapid changes in semimajor axis and incident flux moving toward the future are mainly due to certain $Q_\star$ values being unphysically low and the logarithmic layout of the plots in age, and should not be taken as a sign that we are seeing the system at an especially unique moment of evolution.

5. DISCUSSION

KELT-3b is a typical hot Jupiter. Its host star is among the 20 brightest transiting planet hosts, and so the system provides an opportunity for detailed follow-up observations and analysis. Figure 12 shows the location of KELT-3 in a plot of brightness versus transit depth against other bright transiting planets, demonstrating the potential value of this system for follow-up studies of its atmosphere.

While we are generally able to describe the properties of this system with a self-consistent model, the FUV excess described in §3.2 remains unexplained, and will be a topic of continuing investigation. One intriguing possibility is that it could be an indication of an interaction between the magnetic fields of the star and the planet, causing occasional chromospheric activity, as discussed in Fares et al. (2012). Regardless, we see no signs that the FUV excess negates the overall analysis provided in this paper regarding the properties or existence of KELT-3b.

Aside from its follow-up value as an especially bright transiting planet, KELT-3 itself is nearly identical to the transiting planet host star HAT-P-2 (Pál et al. 2010). Both stars

TABLE 4
MEDIAN VALUES AND 68% CONFIDENCE INTERVALS FOR THE PHYSICAL AND ORBITAL PARAMETERS OF THE KELT-3 SYSTEM

Parameter	Units	Value; $e \neq 0$	Value; $e \equiv 0$, adopted
Stellar Parameters:			
M_*	Mass ($M_\odot$)	$1.274^{+0.062}_{-0.061}$	$1.282^{+0.062}_{-0.060}$
R_*	Radius ($R_\odot$)	$1.453^{+0.078}_{-0.080}$	$1.482^{+0.062}_{-0.064}$
L_*	Luminosity ($L_\odot$)	$3.00^{+0.35}_{-0.34}$	$3.12^{+0.30}_{-0.29}$
ρ_*	Density (cgs)	$0.585^{+0.094}_{-0.074}$	$0.556^{+0.065}_{-0.054}$
$\log g_*$	Surface gravity (cgs)	$4.218^{+0.042}_{-0.038}$	$4.204^{+0.031}_{-0.029}$
$T_{\rm eff}$	Effective temperature (K)	6306^{+48}_{-50}	6304 ± 49
$[{\rm Fe/H}]$	Metallicity	$0.047^{+0.077}_{-0.080}$	$0.048^{+0.079}_{-0.081}$
Planetary Parameters:			
e	Eccentricity	$0.220^{+0.084}_{-0.098}$	$\equiv 0$
ω_*	Argument of periastron (degrees)	-142^{+49}_{-55}	$\equiv 90$
P	Period (days)	$2.7033902^{+0.000010}_{-0.0000099}$	2.703390 ± 0.000010
a	Semi-major axis (AU)	$0.04117^{+0.00066}_{-0.00067}$	$0.04126^{+0.00066}_{-0.00065}$
M_P	Mass (M_J)	$1.418^{+0.072}_{-0.069}$	$1.462^{+0.067}_{-0.066}$
R_P	Radius (R_J)	$1.333^{+0.080}_{-0.081}$	$1.358^{+0.068}_{-0.069}$
ρ_P	Density (cgs)	$0.74^{+0.14}_{-0.11}$	$0.721^{+0.11}_{-0.090}$
$\log g_P$	Surface gravity	$3.296^{+0.048}_{-0.045}$	$3.292^{+0.042}_{-0.039}$
T_{eq}	Equilibrium temperature (K)	1806^{+44}_{-47}	1821^{+35}_{-37}
Θ	Safronov number	$0.0687^{+0.0048}_{-0.0043}$	$0.0692^{+0.0043}_{-0.0039}$
$\langle F \rangle$	Incident flux (10^9 erg s^{-1} cm^{-2})	$2.30^{+0.27}_{-0.28}$	2.50 ± 0.20
RV Parameters:			
T_C	Time of inferior conjunction (BJD_{TDB})	$2456023.471^{+0.044}_{-0.038}$	2456023.446 ± 0.023
T_P	Time of periastron (BJD_{TDB})	$2456024.23^{+0.44}_{-0.42}$	—
K	RV semi-amplitude (m s^{-1})	180.2 ± 5.8	$179.6^{+5.9}_{-5.8}$
$M_P \sin i$	Minimum mass (M_J)	$1.411^{+0.071}_{-0.069}$	1.454 ± 0.066
M_P/M_*	Mass ratio	$0.001064^{+0.000042}_{-0.000041}$	$0.001089^{+0.000039}_{-0.000038}$
u	RM linear limb darkening	$0.6016^{+0.0056}_{-0.0052}$	$0.6017^{+0.0057}_{-0.0053}$
γ_{FIES}	m s^{-1}	-46 ± 26	-46 ± 25
γ_{TRES}	m s^{-1}	$-156.1^{+6.0}_{-5.7}$	-159.3 ± 4.9
$e\cos\omega_*$		$-0.13^{+0.15}_{-0.11}$	—
$e\sin\omega_*$		$-0.10^{+0.15}_{-0.12}$	—
$f(m1,m2)$	Mass function (M_J)	$0.00000158^{+0.00000017}_{-0.00000016}$	$0.00000170^{+0.00000017}_{-0.00000016}$
Primary Transit Parameters:			
R_P/R_*	Radius of the planet in stellar radii	$0.0943^{+0.0010}_{-0.0011}$	$0.0942^{+0.0010}_{-0.0011}$
a/R_*	Semi-major axis in stellar radii	$6.09^{+0.31}_{-0.27}$	$5.99^{+0.23}_{-0.20}$
i	Inclination (degrees)	84.32 ± 0.64	$84.14^{+0.60}_{-0.54}$
b	Impact parameter	$0.637^{+0.073}_{-0.079}$	$0.611^{+0.034}_{-0.042}$
δ	Transit depth	0.00890 ± 0.00020	0.00888 ± 0.00020
T_{FWHM}	FWHM duration (days)	$0.1170^{+0.0042}_{-0.0050}$	0.11419 ± 0.00076
τ	Ingress/egress duration (days)	$0.0191^{+0.0042}_{-0.0035}$	0.0174 ± 0.0014
T_{14}	Total duration (days)	$0.1374^{+0.0062}_{-0.0092}$	0.1316 ± 0.0015
P_T	A priori non-grazing transit probability	$0.140^{+0.026}_{-0.020}$	$0.1513^{+0.0052}_{-0.0054}$
$P_{T,G}$	A priori transit probablity	$0.169^{+0.032}_{-0.024}$	$0.1827^{+0.0065}_{-0.0068}$
$u_{1Sloang}$	Linear Limb-darkening	$0.4674^{+0.0097}_{-0.0087}$	$0.4677^{+0.0098}_{-0.0087}$
$u_{2Sloang}$	Quadratic Limb-darkening	$0.2749^{+0.0043}_{-0.0050}$	$0.2747^{+0.0043}_{-0.0050}$
$u_{1Sloani}$	Linear Limb-darkening	$0.2347^{+0.0054}_{-0.0050}$	$0.2345^{+0.0053}_{-0.0049}$
$u_{2Sloani}$	Quadratic Limb-darkening	$0.3103^{+0.0026}_{-0.0025}$	$0.3104^{+0.0026}_{-0.0024}$
$u_{1Sloanr}$	Linear Limb-darkening	$0.3083^{+0.0064}_{-0.0058}$	$0.3083^{+0.0064}_{-0.0057}$
$u_{2Sloanr}$	Quadratic Limb-darkening	$0.3195^{+0.0021}_{-0.0020}$	$0.3195^{+0.0021}_{-0.0020}$
$u_{1Sloanz}$	Linear Limb-darkening	$0.1835^{+0.0049}_{-0.0045}$	$0.1834^{+0.0047}_{-0.0046}$
$u_{2Sloanz}$	Quadratic Limb-darkening	$0.3015^{+0.0020}_{-0.0025}$	$0.3017^{+0.0020}_{-0.0024}$
Secondary Eclipse Parameters:			
T_S	Time of eclipse (BJD_{TDB})	$2456024.59^{+0.24}_{-0.15}$	2456022.095 ± 0.023
b_S	Impact parameter	$0.523^{+0.11}_{-0.090}$	—
$T_{S,FWHM}$	FWHM duration (days)	$0.1076^{+0.0083}_{-0.011}$	—
τ_S	Ingress/egress duration (days)	$0.0142^{+0.0047}_{-0.0029}$	—
$T_{S,14}$	Total duration (days)	0.122 ± 0.014	—
P_S	A priori non-grazing eclipse probability	$0.172^{+0.020}_{-0.023}$	—
$P_{S,G}$	A priori eclipse probability	$0.208^{+0.024}_{-0.028}$	—

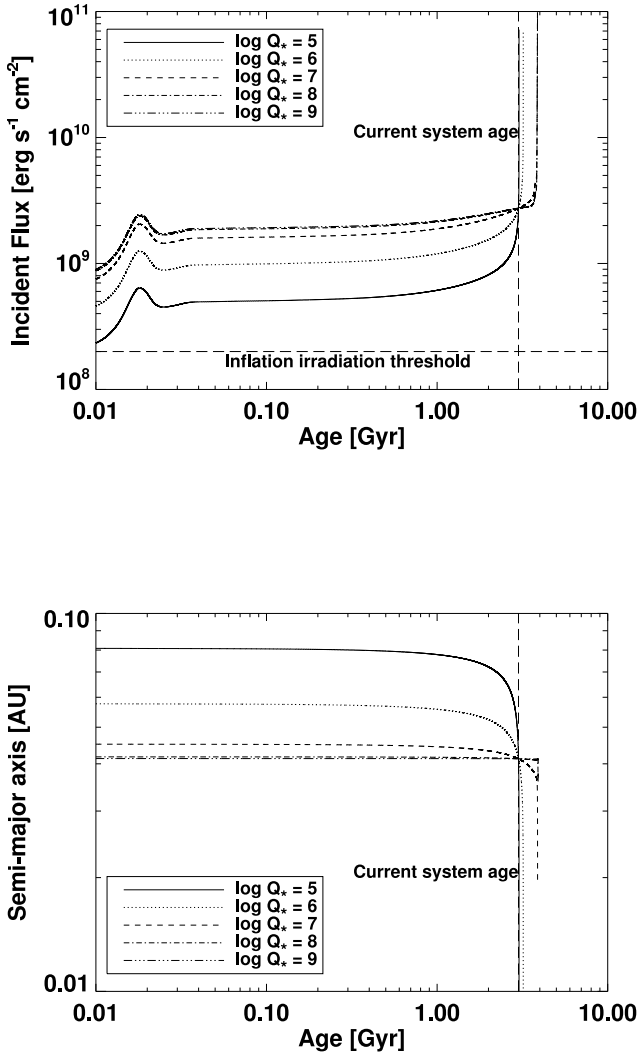

FIG. 11.— Change in incident flux (*top*) and semi-major axis (*bottom*) for KELT-3b, with different test values for Q_* for KELT-3. In all cases the planet has always received more than enough flux from its host to keep the planet irradiated beyond the insolation threshold of 2×10^8 erg s^{-1} cm^{-2} identified by Demory & Seager (2011).

have the same masses, radii, effective temperatures, and surface gravities to within the measurement errors for both stars, and metallicities that differ by only 0.1 dex. The only stellar parameter that differs markedly is the rotational velocity, with HAT-P-2 rotating twice as fast as KELT-3 (20.8 km s^{-1} versus 10.2 km s^{-1}). The availabity of such similar planet hosts can be used to compare different planet formation and evolution theories by comparing how closely exoplanet properties track the properties of their host stars. This particular case offers an especially interesting comparison, since KELT-3b is a relatively typical hot Jupiter, while HAT-P-2b is quite an odd planet companion, with an exceptionally high mass (about $9M_J$) and eccentricity (0.52).

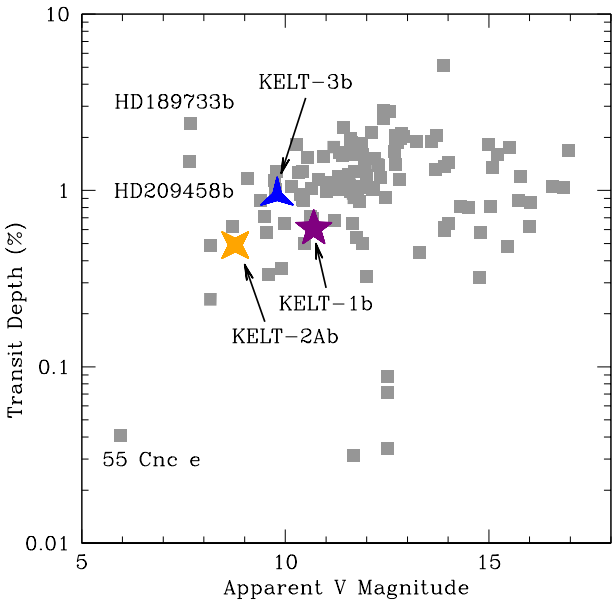

FIG. 12.— Transit depth as a function of the apparent V magnitude of the host star for a sample of transiting systems. KELT-3b is shown as the blue 3-pointed star. All else being equal, objects in the top left provide the best targets for follow-up. The other discoveries from the KELT survey, KELT-1b and KELT-2Ab, are also shown.

We would like to thank additional collaborators on the KELT project, including Bruce Gary, Joao Gregorio, Roberto Zambelli, and Kim McLeod. We would also like to thank Leslie Hebb, Robert Emrich, and Martin Paegert for helpful discussions. Early work on KELT-North was supported by NASA Grant NNG04GO70G. J.A.P. and K.G.S. acknowledge support from the Vanderbilt Office of the Provost through the Vanderbilt Initiative in Data-intensive Astrophysics. E.L.N.J. gratefully acknowledges the support of the National Science Foundation's PREST program, which helped to establish the Peter van de Kamp Observatory through grant AST-0721386. K.G.S. acknowledges the support of the National Science Foundation through PAARE Grant AST-0849736 and AAG Grant AST-1009810. K.A.C. was supported by a NASA Kentucky Space Grant Consortium Graduate Fellowship. Work by B.S.G., J.D.E., and T.G.B. was partially supported by NSF CAREER Grant AST-1056524. The TRES and KeplerCam observations were obtained with partial support from the Kepler Mission through NASA Cooperative Agreement NNX11AB99A with the Smithsonian Astrophysical Observatory (PI: D.W.L.). The Byrne Observatory at Sedgwick (BOS) is operated by the Las Cumbres Observatory Global Telescope Network and is located at the Sedgwick Reserve, a part of the University of California Natural Reserve System. This work has made use of NASA's Astrophysics Data System, the Exoplanet Orbit Database at exoplanets.org, the Extrasolar Planet Encyclopedia at exoplanet.eu (Schneider et al. 2011), and the SIMBAD database operated at CDS, Strasbourg, France.

APPENDIX

INVESTIGATING THE NATURE OF SDSS7J095434 AND ASSOCIATION WITH KELT-3

We perform a number of tests to determine what kind of object SDSS7J095434 is, and to see whether it is physically associated with KELT-3. One approach is to calculate the likelihood that two stars would be located as close together in the sky as KELT-3 and SDSS7J095434. We use the galactic models of Dhital et al. (2010) to create 10^6 realizations of a synthetic galaxy. In each realization, we check first whether two stars are within 3.724 arcseconds of each other in the direction of KELT-3. We find that to be the case in only 2.3% of the time. We also combine the measurement errors of the two distances in quadrature to get 47.8 pc, and check the likelihood that two stars are within that distance of each other in that sky location at the mean distance of $\sim$200 pc. We find that to be the case only 0.1% of the time, further suggesting that SDSS7J095434 is physically associated with KELT-3.

In an additional approach, we attempt to extract the proper motion displacement between KELT-3 and SDSS7J095434 from archival SDSS *z*-band imaging data. The direction of the proper motion of KELT-3 is away from SDSS7J095434, so even though we do not have sufficiently precise archival positions for SDSS7J095434 to measure absolute proper motion, we can measure the changing separation between the two sources.

KELT-3 is saturated in all five SDSS passbands, and SDSS7J095434 is either saturated or compromised in *u*, *g*, *r*, and *i*. However, we identified an SDSS *z*-band image from November 7, 2002, where the neighbor is unaffected by detector saturation. Because KELT-3 itself is still saturated in that image, we could not obtain a conventional centroid for KELT-3. Instead, we fit straight lines to the visible diffraction spikes and take their intersection as the position of KELT-3. Created at the telescope aperture and extending well beyond the core of the stellar PSF, the diffraction spikes can be a reliable position estimator. The resulting uncertainty is at most (very conservatively) ≈ 0.10 pixels (≈ 40 mas).

We then measure the position of SDSS7J095434 on the same image. To avoid biasing the position of SDSS7J095434, we subtract the flux of KELT-3 as cleanly as possible. To work around the saturated core, we estimate and remove flux in concentric annuli about the "spike centroid" described above. This effectively and cleanly removes nearly all the wing flux of KELT-3 from the vicinity of the neighbor. We then compute the neighbor's position using the windowed position estimator from SExtractor (Bertin & Arnouts 1996). We conservatively estimate the position uncertainty as ≈ 0.10 pixels (note: this is the difference in centroid positions with and without removing the local KELT-3 flux).

Given the 10-year baseline between observations and the ≈ 35 mas yr^{-1} proper motion, we would expect a difference of ≈ 350 mas between the SDSS and Keck AO separation measurements, if SDSS7J095434 were in fact an extragalactic source with zero detectable proper motion. The on-sky separation we find in the SDSS image is 3744 ± 56 mas, consistent with the Keck AO separation (3724 mas) to within measured uncertainties, and not consistent with the change in separation expected for a background AGN.

While the test using the archival SDSS image appears reliable, we realize that it is an unorthodox method of astrometric analysis, and we might be ignoring significant systematic effects. However, all lines of evidence support each other, so we therefore conclude that despite the nominally discrepant distances for KELT-3 and SDSS7J095434 based on the SED analysis, and the unexplained FUV excess, the various tests indicate it is likely that SDSS7J095434 is a star, and that it is physically associated with KELT-3, with a projected separation of 663 ± 62 AU, taking the distance to both objects to be 178 ± 16 pc.

We will be able to definitively determine the association of KELT-3 and SDSS7J095434 quite soon. Over one year, the angular separation will increase by about 38 mas if the proper motion of SDSS7J095434 is effectively zero, and a second epoch of AO observations should indicate whether KELT-3 and SDSS7J095434 are moving together and thus likely physically associated.

REFERENCES

Adelman-McCarthy, J. K., & et al. 2009, VizieR Online Data Catalog, 2294, 0

Alard, C. 2000, A&AS, 144, 363

Alard, C., & Lupton, R. H. 1998, ApJ, 503, 325

Assef, R. J., Gaudi, B. S., & Stanek, K. Z. 2009, ApJ, 701, 1616

Baraffe, I., Chabrier, G., & Barman, T. 2008, A&A, 482, 315

Barnes, S. A. 2007, ApJ, 669, 1167

Beatty, T. G., Pepper, J., Siverd, R. J., et al. 2012, arXiv:1206.1592

Bertin, E., & Arnouts, S. 1996, A&AS, 117, 393

Buchhave, L. A., Bakos, G. Á., Hartman, J. D., et al. 2010, ApJ, 720, 1118

Buchhave, L. A., Latham, D. W., Johansen, A., et al. 2012, Nature, 486, 375

Carter, J. A., Winn, J. N., Holman, M. J., et al. 2011, ApJ, 730, 82

Claret, A., & Bloemen, S. 2011, A&A, 529, A75

Collier Cameron, A., Wilson, D. M., West, R. G., et al. 2007, MNRAS, 380, 1230

Copenhagen University, O., Institute, A. O., Cambridge, Uk, & Real Instituto Y Observatorio de La Armada, F. E. S. 2006, VizieR Online Data Catalog, 1304, 0

Cutri, R. M., Skrutskie, M. F., van Dyk, S., et al. 2003, VizieR Online Data Catalog, 2246, 0

Cutri, R. M., & et al. 2012, VizieR Online Data Catalog, 2311, 0

Demarque, P., Woo, J.-H., Kim, Y.-C., & Yi, S. K. 2004, ApJS, 155, 667

Demory, B.-O., & Seager, S. 2011, ApJS, 197, 12

Dhital, S., West, A. A., Stassun, K. G., & Bochanski, J. J. 2010, AJ, 139, 2566

Djupvik, A. A., & Andersen, J. 2010, in "Highlights of Spanish Astrophysics V" eds. J. M. Diego, L. J. Goicoechea, J. I. González-Serrano, & J. Gorgas (Springer: Berlin), p. 211

Eastman, J., Gaudi, B. S., & Agol, E. 2012, Astrophysics Source Code Library, 7001

Fares, R., Donati, J.-F., Moutou, C., et al. 2012, MNRAS, 423, 1006

Findeisen, K., Hillenbrand, L., & Soderblom, D. 2011, AJ, 142, 23

Fűrész, G. 2008, PhD thesis, Univ. Szeged

Gil de Paz, A., Boissier, S., Madore, B. F., et al. 2007, ApJS, 173, 185

Gil de Paz, A., Boissier, S., Madore, B. F., et al. 2009, VizieR Online Data Catalog, 217, 30185

Hartman, J. D., Gaudi, B. S., Holman, M. J., et al. 2008, ApJ, 675, 1254

Hauschildt, P. H., Allard, F., Ferguson, J., Baron, E., & Alexander, D. R. 1999, ApJ, 525, 871

Høg, E., Fabricius, C., Makarov, V. V., et al. 2000, A&A, 355, L27

Kovács, G., Zucker, S., & Mazeh, T. 2002, A&A, 391, 369

Kovács, G., Bakos, G., & Noyes, R. W. 2005, MNRAS, 356, 557

Kupka, F. G., Ryabchikova, T. A., Piskunov, N. E., Stempels, H. C., & Weiss, W. W. 2000, Baltic Astronomy, 9, 590

Kurucz, R. L. 1992, The Stellar Populations of Galaxies, 149, 225

Lucy, L. B., & Sweeney, M. A. 1971, AJ, 76, 544

Martin, D. C., Fanson, J., Schiminovich, D., et al. 2005, ApJ, 619, L1

Pál, A., Bakos, G. Á., Torres, G., et al. 2010, MNRAS, 401, 2665

Pepper, J., Pogge, R. W., DePoy, D. L., et al. 2007, PASP, 119, 923

Richmond, M. W., Droege, T. F., Gombert, G., et al. 2000, PASP, 112, 397

Schlegel, D. J., Finkbeiner, D. P., & Davis, M. 1998, ApJ, 500, 525

Schneider, J., Dedieu, C., Le Sidaner, P., Savalle, R., & Zolotukhin, I. 2011, A&A, 532, A79
Siess, L., Dufour, E., & Forestini, M. 2000, A&A, 358, 593
Siverd, R. J., Beatty, T. G., Pepper, J., et al. 2012, arXiv:1206.1635
Skrutskie, M. F., Cutri, R. M., Stiening, R., et al. 2006, AJ, 131, 1163
Spiegel, D. S., & Madhusudhan, N. 2012, ApJ, 756, 132
Stetson, P. B. 1987, PASP, 99, 191
Torres, G., Andersen, J., & Giménez, A. 2010, A&A Rev., 18, 67
Valenti, J. A., & Piskunov, N. 1996, A&AS, 118, 595
Valenti, J. A., & Fischer, D. A. 2005, ApJS, 159, 141
Wright, E. L., Eisenhardt, P. R. M., Mainzer, A. K., et al. 2010, AJ, 140, 1868
Zacharias, N., Monet, D. G., Levine, S. E., et al. 2004, Bulletin of the American Astronomical Society, 36, 1418